Machine Learning simulations of quad-polarimetric features from dual-polarimetric measurements over sea ice

Katalin Blix, UiT The Arctic University of Norway, katalin.blix@uit.no
Martine M. Espeseth, UiT The Arctic University of Norway, martine.espeseth@uit.no
Torbjørn Eltoft, UiT The Arctic University of Norway, torbjorn.eltoft@uit.no

Abstract

In this paper, we investigated the capabilities of the Gaussian Process Regression (GPR) algorithm in predicting of two quad-polarimetric parameters (relevant for sea ice analysis) from 6-dimensional dual-polarimetric input vectors. The GRP is trained on few hundred samples selected randomly from an image subset, and tested on the entire image. The performance is assessed by visual comparisons, and by quantifying two regression performance statistical measures. The results of the regression showed big variations from scene to scene, and between the estimated output parameters, but the overall assessment is that the method gave surprisingly good correspondence to the real quad-polarimetric parameters.

1 Introduction

Synthetic Aperture Radar (SAR) signatures of sea ice are generally complex, and require careful analysis to enable the extraction of useful and accurate surface information. The interpretation of SAR-derived signatures therefore requires a thorough understanding of the interaction of electromagnetic radiation with the snow, ice, and water layers, and of how this interaction depends on surface properties (roughness and salinity) and imaging parameters (frequency, incidence angle, and polarization). The backscattered signals from sea ice result from a combination of several scattering mechanisms. The relative contributions of rough surface scattering, specular reflections, volume scattering and multiple scattering processes depend on thickness, degree of deformation, size of deformed structures, amount of snow on the ice, salinity, and compactness of the ice fragments [1]. Full-polarimetric (full-pol), also known as quad-polarimetric (quad-pol), SAR observations allow for decomposition of radar signals into contributions from the various scattering mechanisms, and there is on-going research to further develop these decomposition algorithms to provide more accurate information. Quad-pol data can also be transformed into a multitude of polarimetric parameters, some of which giving redundant information, and there are considerable efforts aiming at relating these signal parameters to geophysical properties of sea ice [2].

Full-pol SAR scenes are restricted to narrow swath widths. This is a big drawback and causes severe limitations of these systems when it comes to large-scale mapping of sea ice for operational monitoring. Dual-polarimetric (dual-pol) SAR systems, on the other hand, have large coverage compared to full-pol SARs, but they provide more restricted polarimetric information. However, for large scale monitoring, such as sea ice mapping, dual-pol systems are preferred.

This paper investigates the possibility of extracting more extended polarimetric information from dual-pol data by estimating quad-pol parameters. This we enable by utilising a powerful Machine Learning (ML) model, known as Gaussian Process Regression (GPR). We analyse the regression performance both by visual comparisons, and through statistical error measures between the real quad-pol parameters and the estimated ones.

2 Method

Radar polarimetry deals with the full vector nature of electromagnetic waves. When the electromagnetic wave passes through a medium of changing index of refraction, or when it interact with an object or a target surface and is reflected or scattered, the characteristic information about the reflectivity, shape and orientation of the reflecting body can be obtained by polarimetric analysis of the echoes [3]. This information is only available if the radar system has full polarimetric capability. For the linear polarization basis on a full polarimetric system will enable to measure the backscattered signal in four polarization channels. For example, in the horizontal (H) and vertical (V) polarization basis, the four combinations of channels are {HH,HV,VH,VV}. This is mathematically formulated by means of the Sinclair matrix (also referred to as the scattering matrix), which relates the Jones vector of the backscattered wave to the Jones vector of the incident wave, as shown in (1).

$$\begin{bmatrix} E_h^s \\ E_v^s \end{bmatrix} = \frac{\exp(jkr)}{r} \begin{bmatrix} S_{HH} & S_{HV} \\ S_{VV} & S_{VH} \end{bmatrix} \begin{bmatrix} E_h^i \\ E_v^i, \end{bmatrix}. \quad (1)$$

Dual-pol SAR systems only measures subsets of the Sinclair matrix, for example the set $\{S_{HH}, S_{HV}\}$, or $\{S_{VH}, S_{VV}\}$. Hence, it is not possible to retrieve the

complete polarimetric information from dual-pol data. On the other hand, from the EM scattering theory we know that under certain conditions there are deterministic relationships between the polarimetric channels. Based on this, the objective of this study is to investigate if, and how much, polarimetric information can be retrieved from various dual-pol subsets by utilising an advanced machine learning technique.

2.1 Features

For a given pixel, we try to predict an output quad-pol parameter y from an input feature vector X, generated from dual-pol data. We have chosen the following outputs:

$$y^{(1)} = \frac{\langle |S_{RR} S_{LL}^{\star}| \rangle}{\sqrt{\langle |S_{RR}|^2 \rangle \langle |S_{LL}|^2 \rangle}} \quad (2)$$

$$y^{(2)} = \frac{\langle |S_{HH}|^2 \rangle}{\langle |S_{VV}|^2 \rangle}, \quad (3)$$

where $\langle \cdot \rangle$ indicates spatial averaging for speckle reduction. $y^{(1)}$ has been found to contain information about surface roughness [4], a geophysical property very relevant for sea ice. $y^{(1)}$ is calculated from a linear quad-pol system where we have applied a circular polarization basis on both the transmit and receive channels. $y^{(2)}$ is the co-pol ratio between HH and VV intensities. $y^{(1)}$ and $y^{(2)}$ contain scattering information about the underlaying surface, and are often used in analyses of sea ice polarimetric SAR scenes (e.g., [4] and [5]). Let $\mathbf{C}$, defined as

$$\mathbf{C} = \begin{bmatrix} C_{11} & C_{12} \\ C_{12}{}^{\star} & C_{22} \end{bmatrix}, \quad (4)$$

denote a dual-pol covariance matrix.

In this study we investigate two different dual-pol SAR systems. In System 1, the radar transmits on V and receives on H and V, and its covariance matrix is given by

$$\mathbf{C_1} = \left\langle \begin{bmatrix} |S_{VV}|^2 & S_{VV} S_{VH}^{\star} \\ S_{VH} S_{VV}^{\star} & |S_{VH}|^2 \end{bmatrix} \right\rangle. \quad (5)$$

System 2, transmits on H and receives on V and H, and it can be written by

$$\mathbf{C_2} = \left\langle \begin{bmatrix} |S_{HH}|^2 & S_{HH} S_{HV}^{\star} \\ S_{HV} S_{HH}^{\star} & |S_{HV}|^2 \end{bmatrix} \right\rangle. \quad (6)$$

We generate six input features, $f_1, ..., f_6$, from each covariance matrix, defined by

$$\begin{bmatrix} f_1 \\ f_2 \\ f_3 \\ f_4 \\ f_5 \\ f_6 \end{bmatrix} = \begin{bmatrix} 10\log_{10}(C_{11}) \\ 10\log_{10}(C_{22}) \\ C_{22}/C_{11} \\ |C_{12}|/\sqrt{C_{11}C_{22}} \\ C_{11} - C_{22} \\ (C_{11} - C_{22})/(C_{11} + C_{22}) \end{bmatrix}. \quad (7)$$

These features constitute the input vector $X_k = (f_1, f_2, \cdots, f_6)$ for the multi-looked pixel k. The stack of input and output parameters corresponding to all image pixels define datasets $\mathcal{D}_{ij} = \{\mathbf{X}^j, \mathbf{y}^{(i)}\}$. The inputs $\mathbf{X}^j, j = 1, 2$, are the two input systems defined above. They are two sets of $N \times d$ dimensional matrices created from the six features, where N is the number of observations (pixels), and $d = 6$ is the number of features. The outputs $\mathbf{y}^{(i)}, i = 1, 2$ are $N \times 1$ dimensional vectors representing the two output parameters defined in equations (2) and (3).

2.2 Gaussian Process Regression

Here, we apply regression in the context of estimating a given quad-pol parameter from a set of input features (parameters) generated from dual-pol measurements by fitting a GPR model to a training data set. Let the training set be defined as $\mathcal{D} \equiv \{\mathbf{X}, \mathbf{y}\}$, where $\mathbf{X}$ is a $(N \times d)$-dimensional input matrix, and $\mathbf{y}$ is the corresponding outputs. Then the GPR model is analytically computed as the posterior distribution over the output $\mathbf{y}_*$ [6]

$$\begin{aligned} p(\mathbf{y}_*|\mathbf{X}_*, \mathcal{D}) &= \mathcal{N}(\mathbf{y}_*|\mu_{\text{GP}*}, \sigma^2_{\text{GP}*}) \\ \boldsymbol{\mu}_{\text{GP}*} &= \mathbf{k}_{\mathbf{f}*}^{\top}(\mathbf{K}_{\mathbf{ff}} + \boldsymbol{\sigma}^2\mathbf{I}_n)^{-1}\mathbf{y} = \mathbf{k}_{\mathbf{f}*}^{\top}\boldsymbol{\alpha} \\ \sigma^2_{\text{GP}*} &= \sigma^2 + k_{**} - \mathbf{k}_{\mathbf{f}*}^{\top}(\mathbf{K}_{\mathbf{ff}} + \sigma^2\mathbf{I}_n)^{-1}\mathbf{k}_{\mathbf{f}*}, \end{aligned}$$

where $\mathbf{k}_{\mathbf{f}*}$ is the covariance between the training vector and the test point, $\boldsymbol{\alpha} = (\mathbf{K}_{\mathbf{ff}} + \sigma^2\mathbf{I}_n)^{-1}\mathbf{y}$ is the weight vector of the GP mean and k_{**} is the covariance between the test point with itself.

The covariance prior that we used in this work is the squared exponential kernel function:

$$k(X_m, X_n) = \nu^2 \exp\left(-\frac{1}{2} \sum_{d=1}^{D} \left(\frac{X_m^d - X_n^d}{\lambda_d} \right)^2 \right),$$

where λ_d is the length-scale for the dimension d, and ν is a positive scale factor.

In our case d is 6, and the inputs are the dual-pol parameters defined in equation (7), and the output is the specific quad-pol parameter (see equations (2)-(3)).

2.3 Test scenes

The training dataset was formed by randomly sampling a representative part of the available datasets. Table 1 shows the information about the SAR scenes used, and the number of samples used for training and test. The intensity images (HV) for the two SAR scenes are shown in Figure 1.

The samples for training were drawn from the area indicated with a yellow bounding box in Figure 1 in each of the two scenes. For testing we used all the available data for both scenes, hence the whole images.

Table 1: Description of the test scenes. The Radarsat-2 C-band SAR scenes were acquired in September 2015, the spatial resolution is 5.2×7.6 m, and the swath width is 25×25 km.

	# of samples		Inc.	Center	Averaging
	Training	Test	angle [deg]	coordinates	mask size
S_1	$7, 7 \cdot 10^2$	$7, 7 \cdot 10^5$	23.4-25.3	78°51'N, 6°15'W	9×9
S_2	$1, 2 \cdot 10^2$	$5, 9 \cdot 10^6$	46.8-48.0	78° 2'N, 17°14' W	17×17

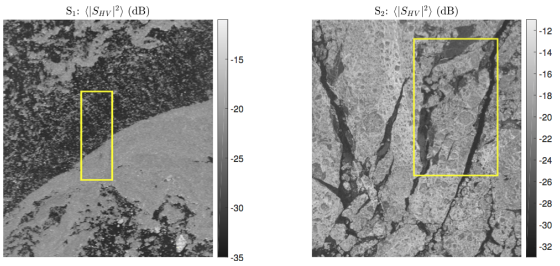

Figure 1: Left; Intensity HV image (in decibel) from the first scene (S_1). Right; Intensity HV image (in decibel) from the second scene (S_2). The yellow bounding box represents the area of the test and training samples.

3 Results

The results are shown in Figures 2 to 5 and in Table 2. Figure 2 shows the results from the first SAR scene (S_1). The left panel in Figure 2 is the true $y^{(1)}$ parameter from the quad-pol data, the center panel is the estimated $\hat{y}^{(1)}$ from the dual-pol input vector for System 1 ({VV, VH}), and the right panel shows the difference between $\hat{y}^{(1)}$ and $y^{(1)}$. Figure 3 shows the results from estimation of the $y^{(2)}$ from System 2 ({HH, HV} using the first SAR scene.

Figures 4 to 5 show the results from the second SAR scene (S_2). Here, Figure 4 shows the results of estimating $y^{(1)}$ from System 2 and Figure 4 for estimation of $y^{(2)}$ from System 1.

Table 2 shows the Normalized Root Mean Squared Errors, the bias, and the Pearson correlation coefficient between output parameters ($y^{(1)}$ and $y^{(2)}$) and the estimated ones ($\hat{y}^{(1)}$ and $\hat{y}^{(2)}$) from the two SAR scenes using the two dual-pol systems. It can be observed that the computed measures show better values for scene 1 than for scene 2. This might be due to a more representative training dataset for scene 1 in comparison to scene 2. However, visual comparison between $\hat{y}^{(i)}$ and the $y^{(i)}$ for scene 2 reveals that using the GPR model might allow to retrieve more information, while removing noise.

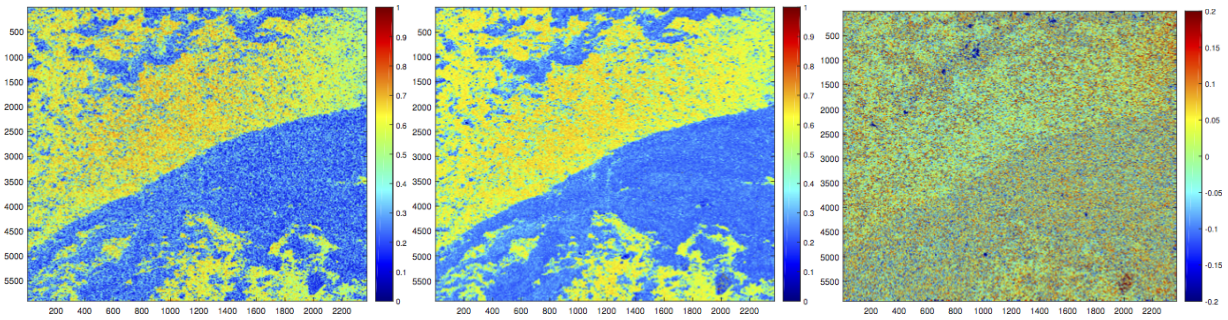

Figure 2: Scene 1: $y^{(1)}$ based on quad-pol input (left panel), estimated parameter ($\hat{y}^{(1)}$) based on dual-pol input vector for System 1 (center panel), and differences ($\hat{y}^{(1)} - y^{(1)}$) between the estimated and the quad-pol parameter (right panel).

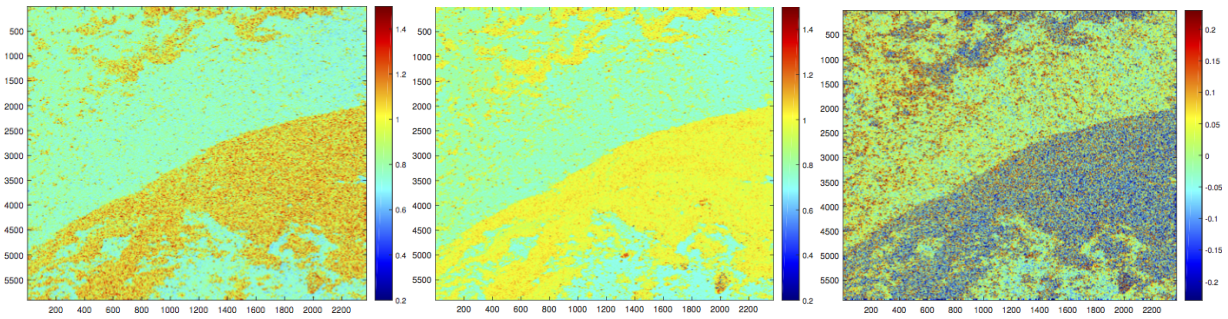

Figure 3: Scene 1: $y^{(2)}$ based on quad-pol input (left panel), estimated parameter ($\hat{y}^{(2)}$) based on dual-pol input vector for System 2 (center panel), and differences ($\hat{y}^{(2)} - y^{(2)}$) between the estimated and the quad-pol parameter (right panel).

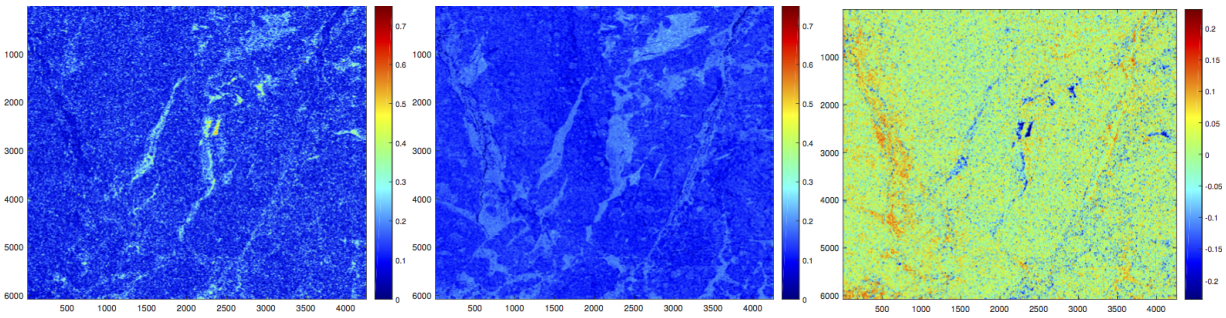

Figure 4: Scene 2: $y^{(1)}$ based on quad-pol input (left panel), estimated parameter ($\hat{y}^{(1)}$) based on dual-pol input vector for System 2 (center panel), and differences ($\hat{y}^{(1)} - y^{(1)}$) between the estimated and the quad-pol parameter (right panel).

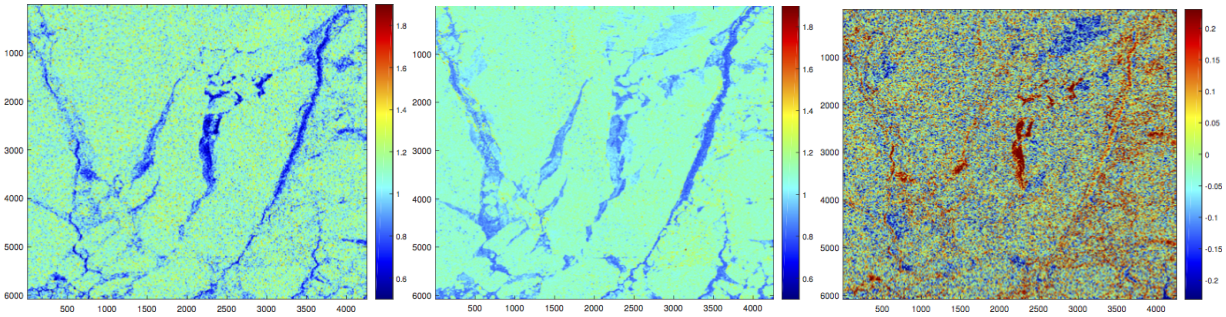

Figure 5: Scene 2: $y^{(2)}$ based on quad-pol input (left panel), estimated parameter ($\hat{y}^{(2)}$) based on dual-pol input vector for System 1 (center panel), and differences ($\hat{y}^{(2)} - y^{(2)}$) between the estimated and the quad-pol parameter (right panel).

Table 2: Computed measures for the test scenes: NRMSE = Normalized Root Mean Squared Errors, Bias = absolute mean errors and R^2 = Pearson correlation coefficient.

Scene 1				
Output	Input system	NRMSE	Bias	R^2
$y^{(1)}$	X_1	0.0104	0.0761	0.8642
$y^{(2)}$	X_1	0.0084	0.0900	0.6704
$y^{(1)}$	X_2	0.0212	0.0687	0.8942
$y^{(2)}$	X_2	0.0136	0.0853	0.7229
Scene 2				
Output	Input system	NRMSE	Bias	R^2
$y^{(1)}$	X_1	0.1159	0.0509	0.3549
$y^{(2)}$	X_1	0.0505	0.1063	0.4803
$y^{(1)}$	X_2	0.0281	0.0500	0.3803
$y^{(2)}$	X_2	0.0476	0.1009	0.5649

4 Conclusion

In this study we investigated the capabilities of an advanced machine learning the Gaussian Process Regression algorithm in estimating quad-pol parameters from dual-pol input feature vectors. The regression algorithm was trained on a few samples (on the order of hundreds) selected randomly from the entire image, and tested on test data comprising the whole scene, i.e., millions of pixels. We generated a 6-dimensional feature input vector from the dual-pol components from a quad-pol Sinclair matrix, and performed regression estimates of quad-pol parameters known to be relevant to sea ice analysis. The performance of the procedure was assessed be visual comparisons, and two regression performance measures using two sea ice scenes. The results show that in some cases the estimation was surprisingly good, whereas in other cases the correspondence with the true quad-pol output was less accurate. However, in all cases, the regression captured real structures in the images. Future studies include improving the GPR model by choosing proper kernel functions that capture more accurately the information in polarimetric data, robust and computationally efficient for big data. In addition, several more SAR scenes will be used, with various incidence angles and sea ice types.

Acknowledgments

Radarsat-2 data were provided by KSAT under the Norwegian-Canadian Radarsat agreement 2015. This research is financed by CIRFA (RCN Grant no. 237906).

References

[1] W. Dierking, A. Carlstrom, and L. M. H. Ulander.: *The effect of inhomogeneous roughness on radar backscattering from slightly deformed sea ice*, IEEE Trans. Geosci. Remote Sens, 35(1):147-159, 1997.

[2] S. V. Nghiem, R. Kwok, S. H. Yueh, and M. R. Drinkwater: *Polarimetric signatures of sea ice: 1. Theoretical model*, J. Geophys. Res., 100(C7):13681-13698, 1995..

[3] W. Boerner: *Basic concepts in radar polarimetry*, Technical report, UIC-ECE Communications, Sensing & Navigation Laboratory, Chicago, IL/USA, 2010.

[4] F. Mattia, T. L Toan, J.-C. Souyris, G. D. Carolis, N. Floury, F. Posa, and G. Pasquariello: *The Effect of Surface Roughness on Multifrequency Polarimetric SAR Data*, IEEE Trans. Geosci. Remote Sens, 35(4):954-996, 1997.

[5] R. Ressel and S. Singha: *Comparing Near Coincident Space Borne C and X Band Fully Polarimetric SAR Data for Arctic Sea Ice Classification* , Remote Sens., 8(3):198, 2016.

[6] C. E. Rasmussen and C. K. I. Williams: *Gaussian Process for Machine Learning*, Cambridge MA: MIT Press.